

Electron Scattering in Gapped Graphene Quantum Dots

Abdelhadi Belouad^a, Youness Zahidi^b, Ahmed Jellal^{*a,c}, Hocine Bahlouli^{c,d}

^a*Theoretical Physics Group, Faculty of Sciences, Chouaib Doukkali University,
PO Box 20, 24000 El Jadida, Morocco*

^b*MATIC laboratory, FPK, Hassan 1 University, Khouribga, Morocco*

^c*Saudi Center for Theoretical Physics, Dhahran, Saudi Arabia*

^d*Physics Department, King Fahd University of Petroleum & Minerals,
Dhahran 31261, Saudi Arabia*

Abstract

Due to Klein tunneling in graphene only quasi-bound states are realized in graphene quantum dots by electrostatic gating. Particles in the quasi-bound states are trapped inside the dot for a finite time and they keep bouncing back and forth till they find their way out. Here we study the effect of an induced gap on the scattering problem of Dirac electrons on a circular electrostatically confined quantum dot. Introducing an energy gap inside the quantum dot enables us to distinguish three scattering regimes instead of two in the case of gapless graphene quantum dot. We will focus on these regimes and analyze the scattering efficiency as a function of the electron energy, the dot radius and the energy gap. Moreover, we will discuss how the system parameters can affect the scattering resonances inside the dot.

PACS numbers: 81.05.ue, 81.07.Ta, 73.22.Pr

Keywords: Graphene, circular quantum dot, scattering, energy gap.

*a.jellal@ucd.ac.ma

1 Introduction

Graphene [1] is a material consisting of a single atomic layer of carbon in sp^2 hybridization. It can be viewed either as a single layer of graphite or an unrolled nanotube. Specifically the electronic properties of graphene are extraordinary. This is why graphene has attracted a lot of interest in fundamental physics for its possible technological applications [1–5]. Graphene can provide a good platform for the study of the electronic properties of a pure two-dimensional system. In graphene the quasi-particles (low-energy excitations) close to the Dirac nodal points behave like mass-less relativistic Dirac fermions with a linear energy dispersion. In addition, graphene presents a variety of exotic electronic properties like electronhole symmetry [2], Klein tunneling [6] and anomalous quantum Hall effect [7].

The equation describing the electronic excitations in graphene is formally similar to the Dirac equation for massless fermions, which travel at a speed of the order of $v_F \approx 10^6 m s^{-1}$ [8, 9]. As a consequence of the pseudo-relativistic dynamics, the massless Dirac fermions have an additional pseudospin degree of freedom. That is the perfect transmission through arbitrarily high and wide rectangular potential barriers or $n-p$ junctions at normal incidence. Unfortunately, the Dirac fermions cannot be confined by electro-static potentials. This is due the Klein tunneling effect [6] and the absence of the gap in the energy spectrum. Thus the realization of the quantum dots is needed to overcome such situation. Recently, alternative strategies have been proposed to confine charged particles by using thin single-layer graphene strips [10,11] or nonuniform magnetic fields [12]. Graphene quantum dots [11, 13, 14] have been recently extensively discussed theoretically as well as from the experimental side [15–20]. It have been studied as potential hosts for spin qubits [21,22], single gate-defined dots [23]. In addition, multiple dots arranged in corrals [22] have been used to model the scattering of Dirac electron waves by impurities or metallic islands placed on a graphene sheet.

Different experimental methods are available to open a gap in graphene band structure, called the Dirac gap [3]. As demonstrated in the experiment, the maximum energy gap could be 260meV due to the sublattice symmetry breaking [24]. It is important to note that the value of the energy gap changes by changing the experimental technique. One of the experimental methods used to open a gap has been demonstrated by controlling the structure of the interface between graphene and ruthenium [25]. Moreover, in graphene grown epitaxially on a SiC substrate an energy gap has been measured [24]. In addition, it has been demonstrated theoretically that an energy gap can be opened by the application of a local strain and/or a chemical methods [3, 26–28].

We study the electron propagation in a circular electrostatically defined quantum dot in monolayer graphene in the presence of an energy gap inside the dot. We identify different scattering regimes depending on the radius, potential and Dirac gap of the dot as well as the electron energy. Then, we determine the scattering coefficients as well as the radial component of the corresponding reflected current. Subsequently, we study the scattering efficiency Q , which is defined as the scattering cross section divided by the geometric cross section of a plane Dirac electron wave hitting on a quantum dot in graphene. The main characteristics of these quantities will be studied in terms of the physical parameter of our system.

The present paper is organized as follows. In section 2, we present a theoretical study of propagation wave plane of electron in a circular quantum dot of monolayer graphene. We give the solutions of the spinors of the Dirac equation corresponding to each region of different scattering parameters. We

use the continuity of the wave functions at the boundary of the dot in order to calculate the scattering coefficients. In section 3, we analyze the scattering efficiency, square modulus of the scattering coefficients and radial component of the far-field. We numerically discuss our results by giving different illustrations. Finally, we close our work by summarizing the main obtained results.

2 Theoretical model

For a Dirac electron in a circular electrostatically defined quantum dot in monolayer graphene with gap $\Delta(r)$, the single-valley Hamiltonian, in the unit system ($\hbar = v_F = 1$), can be written as

$$H = -i\vec{\nabla} \cdot \vec{\sigma} + V(r)\mathbb{1} + \Delta(r)\sigma_z \quad (1)$$

where $\vec{\sigma} = (\sigma_x, \sigma_y, \sigma_z)$ are the Pauli matrices and $\mathbb{1}$ is the 2×2 unit matrix. The applied bias $V(r)$ and $\Delta(r)$ are given by

$$V(r) = \begin{cases} 0, & r > R \\ V, & r \leq R \end{cases}, \quad \Delta(r) = \begin{cases} 0, & r > R \\ \Delta, & r \leq R \end{cases} \quad (2)$$

and R is the quantum dot radius as depicted schematically in Figure 1:

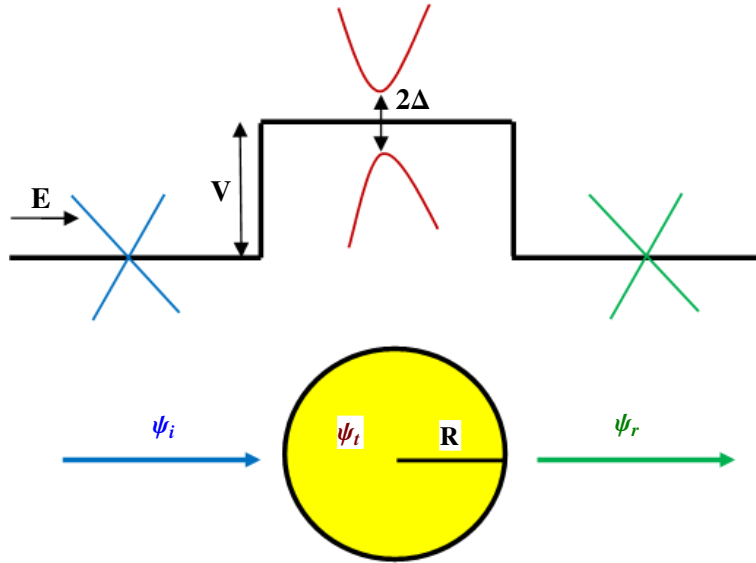


Figure 1: Sketch of Dirac electron scattering for a low energy at a graphene quantum dot in the presence of a gap Δ . The quantum dots are defined electrostatically by applying a constant bias V . For $E < V - \Delta$, the incident ψ_i and reflected ψ_r electron waves reside in the conduction band, while the transmitted ψ_t wave inside the dot corresponds to a state in the valence band.

The geometry presented in Figure 1 suggests to map the system Hamiltonian (1) in the polar coordinates (r, ϕ) as

$$H = \begin{pmatrix} V_+ & e^{-i\phi} \left(-i\frac{\partial}{\partial r} - \frac{1}{r}\frac{\partial}{\partial \phi} \right) \\ e^{i\phi} \left(-i\frac{\partial}{\partial r} + \frac{1}{r}\frac{\partial}{\partial \phi} \right) & V_- \end{pmatrix} \quad (3)$$

where we have defined $V_{\pm} = V \pm \Delta$. One can easily check that H commutes with the total momentum operator $J_z = L_z + \frac{1}{2}\sigma_z$, as consequence the eigenspinors can be chosen to be eigenstates of J_z and therefore they are separated into radial $R^{\pm}(r)$ and angular $\chi(\phi^{\pm})$ parts

$$\psi_m(r, \phi) = \begin{pmatrix} R_m^+(r)\chi_m^+(\phi) \\ R_{m+1}^-(r)\chi_{m+1}^-(\phi) \end{pmatrix} \quad (4)$$

with the eigensates

$$\chi^+(\phi) = \frac{e^{im\phi}}{\sqrt{2\pi}} \begin{pmatrix} 1 \\ 0 \end{pmatrix}, \quad \chi^-(\phi) = \frac{e^{i(m+1)\phi}}{\sqrt{2\pi}} \begin{pmatrix} 0 \\ 1 \end{pmatrix} \quad (5)$$

and $m = 0, \pm 1, \pm 2, \dots$, being the orbital angular momentum quantum number.

In order to get the solutions of the energy spectrum, we have to solve the eigenvalue problem $H\psi_m(r, \phi) = E\psi_m(r, \phi)$ by considering two regions according to Figure 1: outside ($r > R$) and inside ($r \leq R$) the quantum dot. Thus we have an incident wave propagation in the x direction, the reflected wave is an outgoing wave and a transmitted wave inside the quantum dot. Indeed, for $r > R$, we show that the radial parts $R_m^+(r)$ and $R_{m+1}^-(r)$ satisfy two coupled differential equations

$$-i\frac{\partial}{\partial r}R_m^+(r) + i\frac{m}{r}R_m^+(r) = ER_{m+1}^-(r) \quad (6)$$

$$-i\frac{\partial}{\partial r}R_{m+1}^-(r) - i\frac{m+1}{r}R_{m+1}^-(r) = ER_m^+(r) \quad (7)$$

giving rise the second differential equation for $R_m^+(r)$

$$\left(r^2\frac{\partial^2}{\partial r^2} + r\frac{\partial}{\partial r} + r^2E^2 - m^2\right)R_m^+(r) = 0 \quad (8)$$

which having the Bessel functions $J_m(Er)$ as solution. Recalling that, we can expand the incident plane wave as

$$\psi_i(r, \phi) = \frac{e^{ikx}}{\sqrt{2}} \begin{pmatrix} 1 \\ 1 \end{pmatrix} = \frac{1}{\sqrt{2}}e^{ikr\cos\phi} \begin{pmatrix} 1 \\ 1 \end{pmatrix} = \frac{1}{\sqrt{2}}\sum_m i^m J_m(kr)e^{im\phi} \begin{pmatrix} 1 \\ 1 \end{pmatrix}. \quad (9)$$

Using (5), to write the incident spinor as

$$\psi_i(r, \phi) = \sqrt{\pi}\sum_m i^{m+1} \left[-iJ_m(kr)\frac{1}{\sqrt{2\pi}}e^{im\phi} \begin{pmatrix} 1 \\ 0 \end{pmatrix} + J_{m+1}(kr)\frac{1}{\sqrt{2\pi}}e^{i(m+1)\phi} \begin{pmatrix} 0 \\ 1 \end{pmatrix} \right] \quad (10)$$

as well as the reflected one

$$\psi_r(r, \phi) = \sqrt{\pi}\sum_m i^{m+1}a_m \left[-iH_m^{(1)}(kr)\frac{1}{\sqrt{2\pi}}e^{im\phi} \begin{pmatrix} 1 \\ 0 \end{pmatrix} + H_{m+1}^{(1)}(kr)\frac{1}{\sqrt{2\pi}}e^{i(m+1)\phi} \begin{pmatrix} 0 \\ 1 \end{pmatrix} \right] \quad (11)$$

where $H_m^{(1)}(kr)$ are the Hankel function of the first kind, a_m are the scattering coefficients and the wave number $k = E$. Now for the second case $r \leq R$, we have

$$-i\left(\frac{\partial}{\partial r} - \frac{m}{r}\right)R_m^+(r) = (E - V_-)R_{m+1}^-(r) \quad (12)$$

$$-i\left(\frac{\partial}{\partial r} + \frac{m+1}{r}\right)R_{m+1}^-(r) = (E - V_+)R_m^+(r) \quad (13)$$

which allow to obtain

$$\left(r^2 \frac{\partial^2}{\partial^2 r} + r \frac{\partial}{\partial r} + r^2 \eta^2 - m^2 \right) R_m^+(r) = 0 \quad (14)$$

where we have set $\eta^2 = (E - V)^2 - \Delta^2$. This gives the transmitted spinor as

$$\psi_t(r, \phi) = \sqrt{\pi} \sum_m i^{m+1} b_m \left[-i J_m(\eta r) \frac{1}{\sqrt{2\pi}} e^{im\phi} \begin{pmatrix} 1 \\ 0 \end{pmatrix} + \mu J_{m+1}(\eta r) \frac{1}{\sqrt{2\pi}} e^{i(m+1)\phi} \begin{pmatrix} 0 \\ 1 \end{pmatrix} \right] \quad (15)$$

with $\mu = \sqrt{\frac{E-V_+}{E-V_-}}$ and b_m are the scattering coefficients. Later on, we will see the above results can be used to study the scattering of Dirac electrons in our system.

3 Scattering problem

To study the scattering problem of our system, we need first to determine the scattering coefficients a_m and b_m . This can be done by requiring the eigenspinors continuity at the boundary $r = R$, $\psi_i(R) + \psi_r(R) = \psi_t(R)$, to end up with two conditions

$$J_m(kR) + a_m H_m^{(1)}(kR) = b_m J_m(\eta R) \quad (16)$$

$$J_{m+1}(kR) + a_m H_{m+1}^{(1)}(kR) = \mu b_m J_{m+1}(\eta R) \quad (17)$$

which can be solved to obtain a_m and b_m

$$a_m = \frac{-J_m(\eta R) J_{m+1}(kR) + \mu J_{m+1}(\eta R) J_m(kR)}{J_m(\eta R) H_{m+1}^{(1)}(kR) - \mu J_{m+1}(\eta R) H_m^{(1)}(kR)} \quad (18)$$

$$b_m = \frac{J_m(kR) H_{m+1}^{(1)}(kR) - J_{m+1}(kR) H_m^{(1)}(kR)}{J_m(\eta R) H_{m+1}^{(1)}(kR) - \mu J_{m+1}(\eta R) H_m^{(1)}(kR)}. \quad (19)$$

According to the Hamiltonian (1), the component of the current density is $\vec{j} = \psi^\dagger \vec{\sigma} \psi$ where inside the quantum dot $\psi = \psi_t$ and outside $\psi = \psi_i + \psi_r$. The radial component of the current reads as

$$j_r = \vec{j} \cdot \vec{e}_r = \psi^\dagger (\sigma_x \cos \phi + \sigma_y \sin \phi) \psi \quad (20)$$

or equivalently

$$j_r = \psi^\dagger \begin{pmatrix} 0 & \cos \phi - i \sin \phi \\ \cos \phi + i \sin \phi & 0 \end{pmatrix} \psi. \quad (21)$$

Thus, the radial current for the reflected wave takes the form

$$j_r^r = \frac{1}{2} \sum_{m=0}^{m=\infty} A_m(kr) \begin{pmatrix} 0 & e^{-i\phi} \\ e^{-i\phi} & 0 \end{pmatrix} \sum_{m=0}^{m=\infty} B_m(kr) \quad (22)$$

where different coefficients are given by

$$A_m(kr) = (-i)^{m+1} \left[i H_m^{(1)*}(kr) \begin{pmatrix} a_m^* e^{-im\phi} & a_{-(m+1)}^* e^{im\phi} \\ + H_{m+1}^{(1)*}(kr) \begin{pmatrix} a_{-(m+1)}^* e^{i(m+1)\phi} & a_m^* e^{-i(m+1)\phi} \end{pmatrix} \right] \quad (23)$$

$$B_m(kr) = i^{m+1} \left[-i H_m^{(1)}(kr) \begin{pmatrix} a_m e^{im\phi} \\ a_{-(m+1)} e^{-im\phi} \end{pmatrix} + H_{m+1}^{(1)}(kr) \begin{pmatrix} a_{-(m+1)} e^{-i(m+1)\phi} \\ a_m e^{i(m+1)\phi} \end{pmatrix} \right]. \quad (24)$$

The asymptotic behavior of the Hankel function of the first kind for $kr \gg 1$, gives the approximate function

$$H_m(kr) \simeq \sqrt{\frac{2}{\pi kr}} e^{i(kr - \frac{m\pi}{2} - \frac{\pi}{4})} \quad (25)$$

leads to a reduced form of (22)

$$j_r^r(\phi) = \frac{4}{k\pi r} \sum_{m=0}^{m=\infty} |c_m|^2 [\cos(2m+1)\phi + 1] \quad (26)$$

where we have defined $|c_m|^2 = \frac{1}{2}(|a_m|^2 + |a_{-(m+1)}|^2)$. This reflected current density will be used to determine two interesting quantities.

Let us investigate some interesting quantities related to our system and underline their basic features. Indeed we can use (26) in the limit $kr \rightarrow \infty$ to calculate the scattering cross section σ defined by

$$\sigma = I_r^r / (I^i / A_u) \quad (27)$$

where I_r^r is the total reflected flux through a concentric circle and I^i / A_u is the incident flux per unit area. From our results, we show that I_r^r takes the form

$$I_r^r = \int_0^{2\pi} J_r^r(\phi) r d\phi = \frac{8}{k} \sum_{m=0}^{m=\infty} |c_m|^2 \quad (28)$$

while for the incident wave (9), we end up with $I^i / A_u = 1$. To go deeply in our study for the scattering problem for a plane Dirac electron for different size of the circular quantum dot, we analyze the scattering efficiency Q . This is given as the ratio between the scattering cross section and the geometric cross section

$$Q = \frac{\sigma}{2R} = \frac{4}{kR} \sum_{m=0}^{m=\infty} |c_m|^2. \quad (29)$$

Having settled the scattering efficiency and the radial current, we proceed next to numerically compute these quantities in terms of different physical parameters of our system. This will help us to understand the effect of the energy gap and the dot radius on the scattering in the quantum dot.

4 Results and discussions

To allow for a suitable interpretation of the scattering cross section we have defined the scattering efficiency Q , which will be numerically computed under various conditions. Before doing so, we define different scattering regimes. Indeed, according to the electron energy E being less or above V_{\pm} , we define three regimes referred to $E < V_-$, $V_- < E < V_+$ and $V_+ < E$. Note that, the second regime is a consequence of the introduction of an energy gap inside the dot. This is in contrast with the case of gapless graphene quantum dot [29] where there is only two regimes.

Numerical results for the scattering efficiency Q versus the quantum dot radius R for different values of the incident energy E , with some choices of the potential height V and the energy gap Δ , are shown in Figure 2 for three different scattering regimes. Figure 2(a) corresponds to $E < V_-$, in this regime the region outside the dot of radius R contains electrons in the conduction band, whereas

the region inside the dot contains holes in the valence band where there is only evanescent waves. From this Figure, it is clearly seen that, for small energy, when R is small (close to 0), Q is still null. By increasing the dot radius, Q shows an oscillatory behavior where the amplitude decreases by increasing R and sharp peaks emerge. However, by increasing E the oscillations become relatively smooth. Moreover, the scattering resonances appear, which are due to the excitation of normal modes in the quantum dot. We present in Figure 2(b) the scattering efficiency Q versus the quantum dot radius R for the electronic state inside the quantum dot around the Dirac point where $V_- < E < V_+$. We observe that when the dot radius is close to 0, Q is null. Note that in this regime there are no available states inside the dot. In addition, by increasing R , the scattering efficiency Q increase almost linearly up to a specific value of R above which an oscillatory behavior sets in. The amplitude of the oscillations decreases by increasing E . However, for larger R these oscillations are relatively damped. For the third regime, the results are shown in Figure 2(c) where the regions outside and inside the dot have electrons in the conduction band. From this Figure, we can see clearly that when R is close to zero the results are similar to those corresponding to $V_- < E < V_+$. But, by increasing R and for the three values of the energy, the three curves are superimposed and increase linearly up to a specific value of R then Q shows an oscillatory behavior. The amplitude of the oscillations depends on the values of the energy E , it increases as long as E increased.

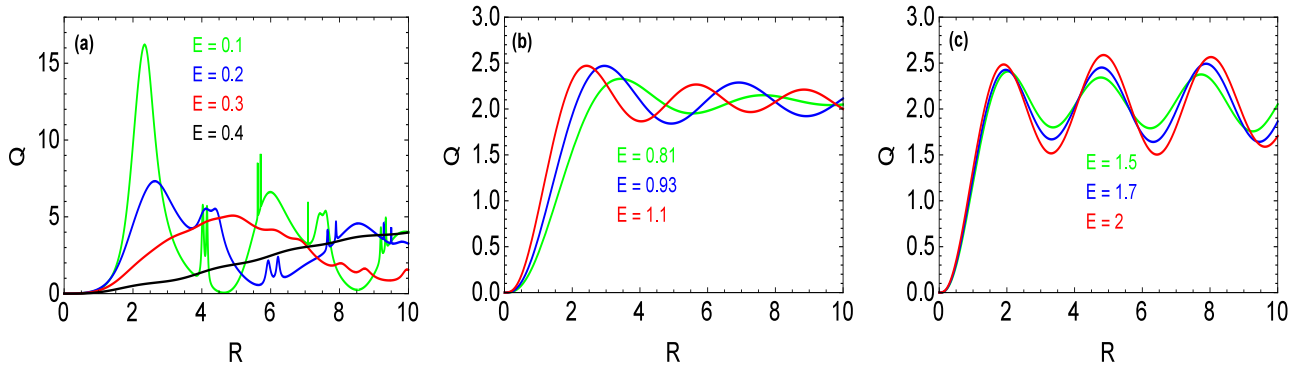


Figure 2: Scattering efficiency Q versus the quantum dot radius R for different values of the incident energy E , with the potential $V = 1$ and gap $\Delta = 0.2$. (a): $E < V_-$, (b): $V_- < E < V_+$, (c): $V_+ < E$.

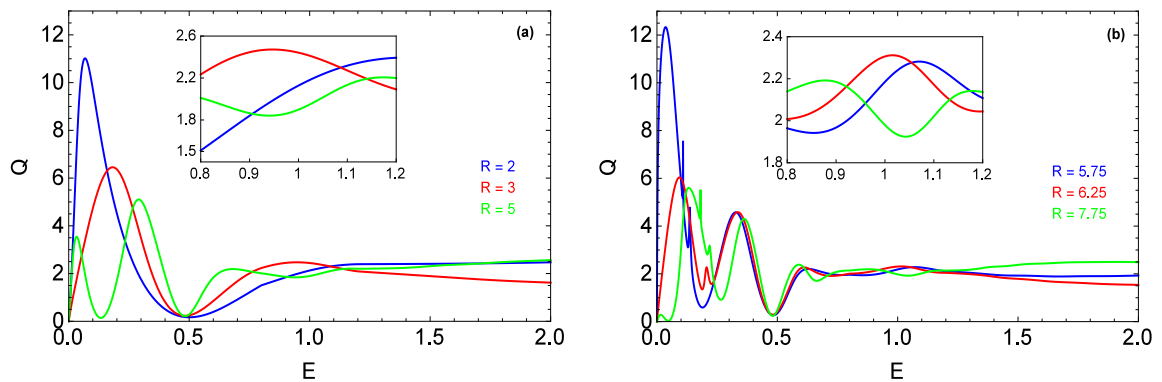


Figure 3: Scattering efficiency Q versus the energy E of the incident electron for different size of the quantum dot radius R , with $\Delta = 0.2$ and $V = 1$. (a): $R = 2, 3, 5$, (b): $R = 5.75, 6.25, 7.75$.

To further analyze the scattering in the three regimes, we plot in Figure 3 the scattering efficiency Q as function of incident energy E for different size of the quantum dot radius R . In the first regime ($E < V_-$), we can clearly see that for small values of R , Q is zero for $E = 0$ and by increasing E , Q shows broad maxima. The maximum of Q decreases as long as R is increased. However for large R , Q also show broad maxima and we observe the appearance of peaks emerging with damped oscillations. These sharp peaks are due to the resonant excitation of normal modes of the quantum dot, which are presents even if $\Delta = 0$ [29]. The results for the second regime ($V_- < E < V_+$) are shown in the inset of Figure 3 where Q shows an oscillatory behavior with small amplitude. In the third regime, we show that the oscillations are damped and Q remains constant even if E increases.

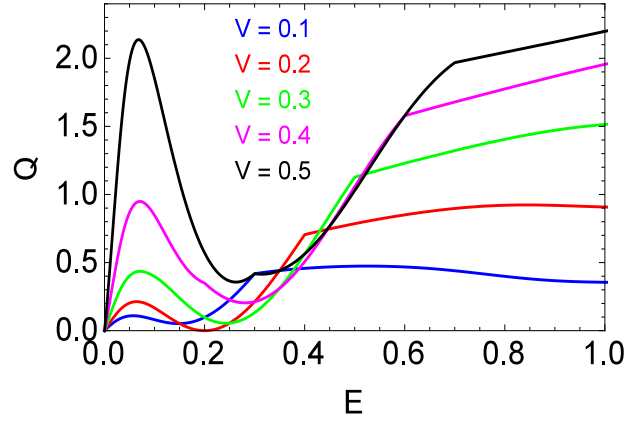


Figure 4: Scattering efficiency Q versus the energy E of the incident electron for different values of the potential height ($V = 0.1, 0.2, 0.3, 0.4, 0.5$) with $\Delta = 0.2$ and $R = 3$.

In order to show how the potential V affects the scattering efficiency, we plot in Figure 4 Q as function of the energy for different values of the potential V with $\Delta = 0.2$ and $R = 3$. By increasing E , Q shows broad maxima, which depend on the value of V . In fact, by increasing V , the maxima increase. For large values of E , Q undergoes an almost linear increase, specially when $E > V + \Delta$.

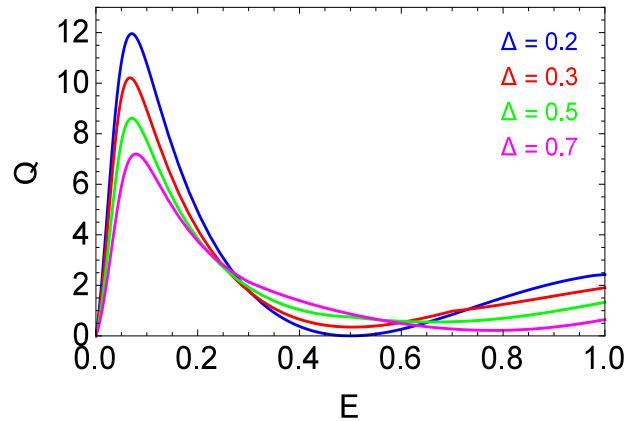


Figure 5: Scattering efficiency Q versus the energy E of the incident electron for different values of the gap ($\Delta = 0.1, 0.3, 0.5, 0.7$) with $V = 1$ and $R = 2$.

Figure 5 shows the scattering efficiency Q as a function of the energy E . It has been performed using $V = 1$, $R = 2$ and taking different values for the gap ($\Delta = 0.1, 0.3, 0.5, 0.7$). We notice that for $E = 0$, Q is zero whatever the values of Δ and R . By increasing E , Q increases until it reaches a maximum value with different amplitudes, then decreases to a minimum value and starts to increase again. By increasing Δ , we observe that the maxima decrease and when $E > V + \Delta$ Q remains constant even if the energy E increases.

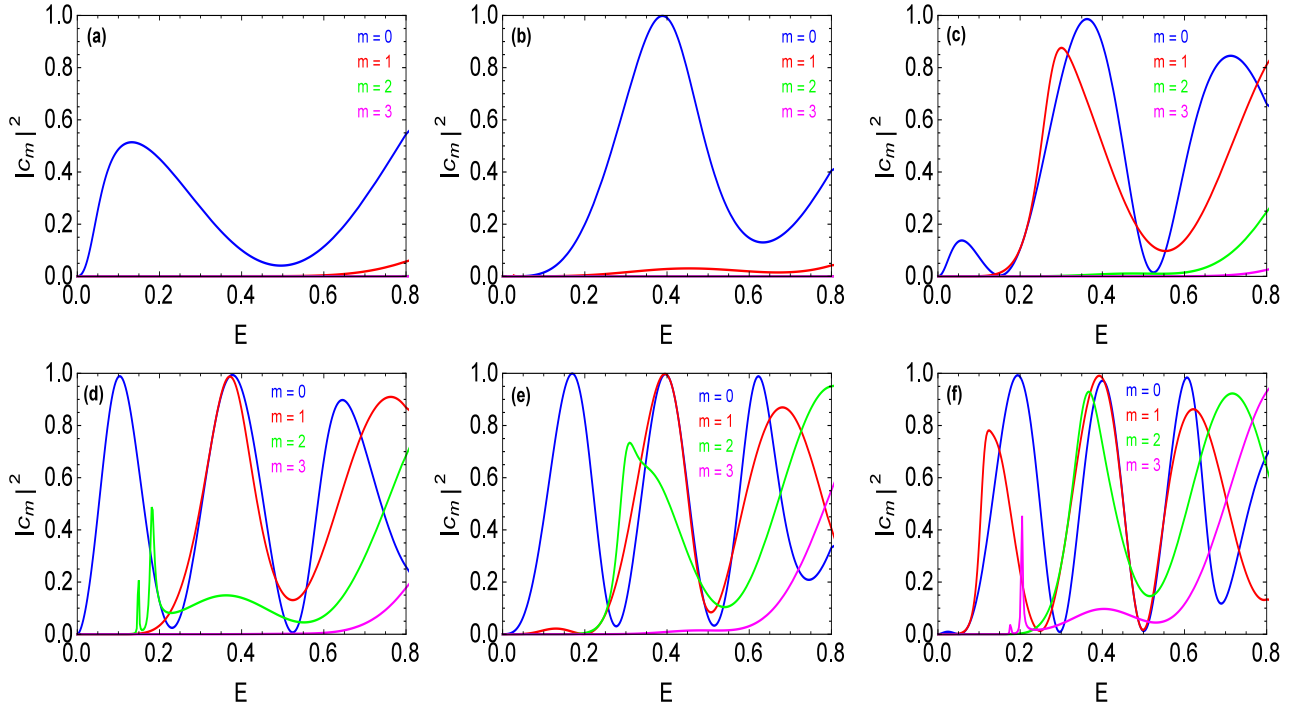


Figure 6: Square modulus of the scattering coefficients $|c_m|^2$ for $m = 0, 1, 2, 3$ versus the energy E , with $V = 1$, $\Delta = 0.2$ and for six values of the quantum dot radius R : $R = 2$ panel (a), $R = 4$ panel (b), $R = 5$ panel (c), $R = 6$ panel (d), $R = 7$ panel (e) and $R = 7.75$ panel (f).

In Figure 6, we plot the square modulus of the scattering coefficients $|c_m|^2$ for $m = 0, 1, 2, 3$ as function of the energy E , for $V = 1$, $\Delta = 0.2$ with (a): $R = 2$, (b): $R = 4$, (c): $R = 5$, (d): $R = 6$, (e): $R = 7$, (f): $R = 7.75$. From these Figures, we observe that for zero or close to zero energy all scattering coefficients are zero except the one corresponding to $m = 0$. By increasing E , we can clearly observe the contribution of the scattering coefficients of higher orders *i.e.* $m = 1, 2, 3$. By increasing E , $|c_m|^2$ restores an oscillatory behavior. As compared to the results for zero gap [29], we notice that the presence of an gap increases the number of oscillations. Moreover, one can see that for some values of E , $|c_m|^2$ presents sharp peaks. These resonances associated with normal modes of the quantum dot lead to the existence of sharp peaks in Figure 3, which is similar to that observed for zero gap [29].

The current is defined by $j = \psi^\dagger \sigma \psi$, where $\psi = \psi_i + \psi_r$ outside and $\psi = \psi_t$ inside the gated dot region. As a result of that the far-field radial component of the reflected current $j_r^r(\phi)$ characterizes the angular scattering is given by

$$j_r^r(\phi) \sim |c_m|^2 [\cos((2m+1)\phi) + 1]. \quad (30)$$

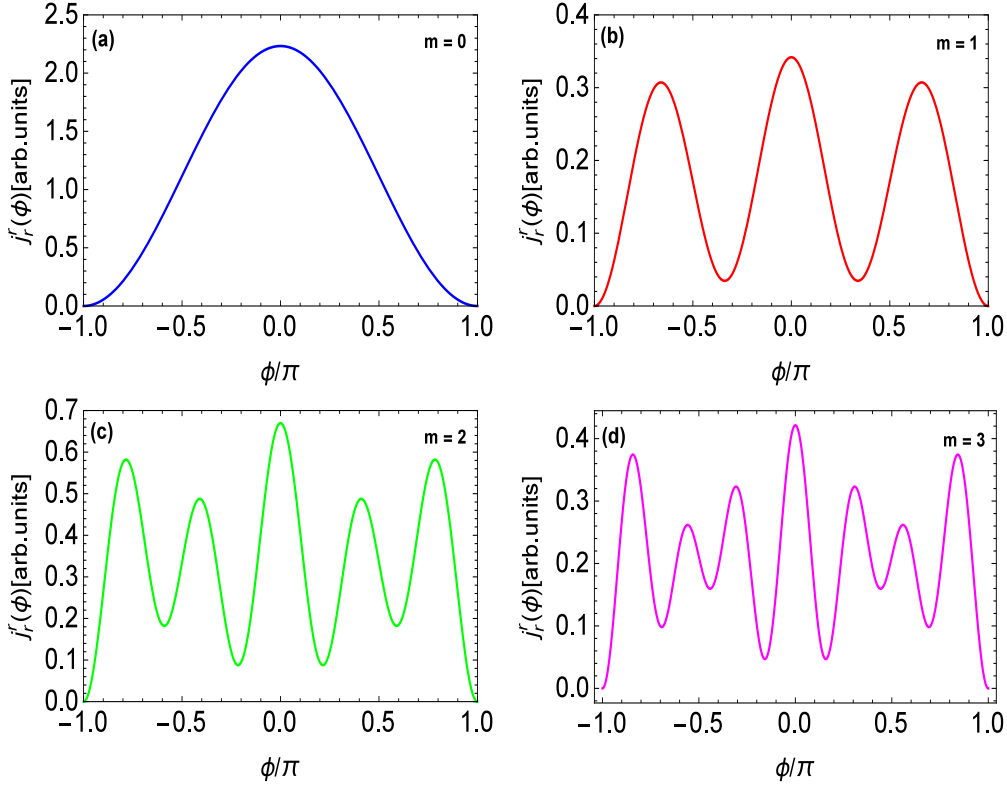


Figure 7: Radial component of the far-field scattered current j_r^r as a function of the angle ϕ for $\Delta = 0.2$ and $V = 1$. (a): $E = 0.0704$ and $R = 3$, (b): $E = 0.484$ and $R = 4$, (c): $E = 0.67$ and $R = 7.75$, (d): $E = 0.99$ and $R = 6.25$.

In Figure 7, we plot the angular characteristic of the reflected radial component as a function of the angle ϕ . It shows that only forward scattering is preferred (no backscattering) when $\varphi = \pm\pi$. In addition, for the mode c_0 (panel (a)) only forward scattering is favored. While for higher modes more preferred scattering directions emerge. Thereby, for $m = 1$ (panel (b)) three preferred scattering directions. However, for $m = 2$ (panel (c)) five preferred scattering directions and for $m = 3$ (panel (d)) seven preferred scattering directions. In general, each mode has $(2m + 1)$ preferred scattering directions observable but with different amplitudes. For small electron energies the mode ($m = 0$) is relatively broad compared to the sharp resonances of higher modes. Resonant scattering through one of the normal modes is also reflected in the electron density profile in the vicinity of the quantum dot.

5 Conclusion

We have studied the scattering problem of an electron plane wave on a circular electrostatically confined quantum dot in monolayer graphene with gap and compared our results with those obtained for zero gap situation [29]. Different scattering regimes were investigated as a function of the radius R of the quantum dot, electrostatic potential V , energy gap Δ and incident electron energy E . We have found that scattering efficiency Q , for $E > V_+$ increases with increasing R , first almost linearly up to a specific value of R then showed an oscillatory behavior. The amplitude of the oscillations increased with increasing E . When $V_- < E < V_+$, Q showed the same behavior as for $E > V_+$, but

the oscillations are relatively damped. However, for $E < V_-$, Q showed an oscillatory behavior where their amplitudes decrease by increasing R . Moreover, sharp peaks emerge, which were due to the resonant excitations of the normal modes of the quantum dot.

The scattering efficiency Q was also computed numerically as a function of the energy by choosing different values of the potential V , quantum dot radius R and gap Δ . We have observed that by increasing E , Q shows broad maxima, which depend on the value of V . For larger values of E , Q undergoes an almost linear increase specially when $E > V + \Delta$. However, when $E > V + \Delta$, Q remains constant even if the energy E increases. It has been seen that the square modulus of Q is zero in the vicinity of $E = 0$, except for $m = 0$ mode. In addition, by increasing the energy the scattering coefficients shows an oscillatory behavior. For the angular characteristic of the reflected radial component, we found that each mode has $(2m + 1)$ preferred scattering directions observable with different amplitudes.

Acknowledgment

The generous support provided by the Saudi Center for Theoretical Physics (SCTP) is highly appreciated by all authors. HB and AJ acknowledges partial support by King Fahd University of petroleum and minerals under the theoretical physics research group project RG171007-1 and -2.

References

- [1] K. S. Novoselov, A. K. Geim, S. V. Morozov, D. Jiang, Y. Zhang, S. V. Dubonos, I. V. Grigorieva and A. A. Firsov, *Science* 306, 666 (2004).
- [2] A. H. Castro Neto, F. Guinea, N. M. R. Peres, K. S. Novoselov and A. K. Geim, *Rev. Mod. Phys.* 81, 109 (2009).
- [3] D. S. L. Abergel, V. Apalkov, J. Berashevich, K. Ziegler and T. Chakraborty, *Adv. Phys.* 59, 261 (2010).
- [4] V. N. Kotov, B. Uchoa, V. M. Pereira, F. Guinea and A. H. Castro Neto, *Rev. Mod. Phys.* 84, 1067 (2012).
- [5] F. Bonaccorso, A. Lombardo, T. Hasan, Z. Sun, L. Colombo and A. C. Ferrari, *Mat. Today* 15, 564 (2012).
- [6] M. I. Katsnelson, K. S. Novoselov and A. K. Geim, *Nat. Phys.* 2, 620 (2006).
- [7] V. P. Gusynin and S. V. Sharapov, *Phys. Rev. Lett.* 95, 14 (2005).
- [8] G. W. Semenoff, *Phys. Rev. Lett.* 53, 2449 (1984).
- [9] D. P. DiVincenzo and E. J. Mele. *Phys. Rev. B* 29, 1685 (1984).
- [10] N. M. R. Peres, A. H. Castro Neto and F. Guinea, *Phys. Rev. B* 73, 241403 (2006) .
- [11] P. G. Silvestrov and K. B. Efetov, *Phys. Rev. Lett.* 98, 016802 (2007).

- [12] C. Berger, Z. Song, X. Li, X. Wu, N. Brown, C. Naud, D. Mayou, T. Li, J. Hass, A. N. Marchenkov, E. H. Conrad, P. N. First and W. A. de Heer, *Science* 312, 1191 (2006).
- [13] T. Chakraborty, *Quantum Dots* (Amsterdam: Elsevier) (1999).
- [14] A. Matulis and F. M. Peeters, *Phys. Rev. B* 77, 115423 (2008).
- [15] A. Belouad, Y. Zahidi and A. Jellal, *Mater. Res. Express* 3, 055005 (2016).
- [16] A. Belouad, A. Jellal and Y. Zahidi, *Phys. Lett. A* 380, 773 (2016).
- [17] P. Recher, J. Nilsson, G. Burkard and B. Trauzettel, *Phys. Rev. B* 79, 085407 (2009).
- [18] S. Schnez, F. Molitor, C. Stampfer, J. Güttinger, I. Shorubalko, T. Ihn and K. Ensslin, *Appl. Phys. Lett.* 94, 012107 (2009).
- [19] J. Güttinger, C. Stampfer, T. Frey, T. Ihn and K. Ensslin, *Phys. Status Solidi B* 246, 2553 (2009).
- [20] G. A. Steele, G. Gotz and L. P. Kouwenhoven, *Nat. Nanotech.* 4, 363 (2009).
- [21] B. Trauzettel, D. V. Bulaev, D. Loss and G. Burkard, *Nat. Phys.* 3, 192 (2007).
- [22] P. Recher and B. Trauzettel, *Nanotech.* 21, 302001 (2010).
- [23] M. Hentschel and F. Guinea, *Phys. Rev. B* 76, 115407 (2007).
- [24] S. Y. Zhou, G.-H. Gweon, A. V. Fedorov, P. N. First, W. A. deHeer, D.-H. Lee, F. Guinea, A. H. Castro Neto and A. Lanzara, *Nat. Mater.* 6, 770 (2007).
- [25] C. Enderlein, Y. S. Kim, A. Bostwick, E. Rotenberg and K. Horn, *New. J. Phys.* 12, 033014 (2010).
- [26] G. Giovannetti, P. A. Khomyakov, G. Brocks, P. J. Kelly and J. van den Brink, *Phys. Rev. B* 76, 073103 (2007).
- [27] R. P. Tiwari and D. Stroud, *Phys. Rev. B* 79, 205435 (2009).
- [28] R. M. Ribeiro, N. M. R. Peres, J. Coutinho and P. R. Briddon, *Phys. Rev. B* 78, 075442 (2008).
- [29] C. Schulz, R. L. Heinisch and H. Fehske, *Quantum Matt.* 4, 346 (2015).